

# *Ab initio* study of spin-dependent transport in carbon nanotubes with iron and vanadium adatoms

Joachim A. Fürst,<sup>1,2,\*</sup> Mads Brandbyge,<sup>1</sup> Antti-Pekka Jauho,<sup>1,3</sup> and Kurt Stokbro<sup>4</sup>

<sup>1</sup>*MIC – Department of Micro and Nanotechnology, NanoDTU,*

*Technical University of Denmark, DK-2800 Kongens Lyngby, Denmark*

<sup>2</sup>*Atomistix A/S, c/o Niels Bohr Institute, 2100 Copenhagen, Denmark*

<sup>3</sup>*Laboratory of Physics, Helsinki University of Technology, P. O. Box 1100, FI-02015 HUT, Finland*

<sup>4</sup>*Department of Computer Science, Universitetsparken 1, DK-2100 Copenhagen Ø, Denmark*

(Dated: May 6, 2019)

We present an *ab initio* study of spin dependent transport in armchair carbon nanotubes with transition metal adsorbates, iron or vanadium. We neglect the effect of tube curvature and model the nanotube by graphene with periodic boundary conditions. A density functional theory based nonequilibrium Green's function method is used to compute the electronic structure and zero-bias conductance. The presence of the adsorbate causes a strong scattering of electrons of one spin type only. The scattering is shown to be due to coupling of the two armchair band states to the metal 3d orbitals with matching symmetry causing Fano resonances appearing as dips in the transmission function. The spin type (majority/minority) being scattered depends on the adsorbate and is explained in terms of *d*-state filling. The results are qualitatively reproduced using a simple tight-binding model, which is then used to investigate the dependence of the transmission on the nanotube width. We find a decrease in the width of the transmission dip as the tube-size increases.

PACS numbers: 73.63.Fg, 73.63.-b

## I. INTRODUCTION

Various carbon structures have attracted considerable attention in the last decade or so, due to their potential use within future nanodevices<sup>1</sup>. Graphene, the single-atom thick two-dimensional sheet of graphite is the basis for many carbon materials. Rolling up such a sheet creates the one-dimensional single-walled carbon nanotube (SWNT) and wrapping up a sheet makes 0D fullerenes. These materials have a wide range of remarkable electronic properties. Recently graphene ribbons – cut graphene sheets – were used to make the first transistor carved in graphene<sup>2</sup> which is stable at room temperature.

Not only pushing the limits within electronics, these carbon materials may lay the ground for the emerging field of spintronics<sup>3,4,5</sup>, where the functionality of the device is based on the spin degree of freedom. While graphene and SWNT's are not inherently magnetic, introducing defects<sup>6,7,8</sup>, impurities or boundaries<sup>9,10</sup> may alter this fact. In recent years several studies have been carried out on SWNT/graphene - transition metal adatom systems. First principles calculations have been employed to determine equilibrium geometries and magnetic properties: Fagan *et al.* reported electronic structure studies on single iron<sup>11,12,13</sup> and manganese adatoms<sup>11,12</sup> on zigzag SWNT's showing a total magnetic moment of the systems and in most cases a magnetisation of the tube itself. A similar earlier study with additional transition metal elements on graphene was published by Duffy *et al.*<sup>14</sup> reaching similar conclusions. Manganese dimers, trimers and wires on zigzag SWNT's<sup>12</sup> exhibit magnetic moments close to free manganese. Yang *et al.*<sup>15</sup> have proposed that iron and cobalt coated and filled

SWNT's can work as spintronic devices demonstrating a spin polarisation close to 90 % at the Fermi level as well as considerable magnetic moments. Interestingly, both semiconducting and metallic SNWT's showed high spin polarisation. Kang *et al.*<sup>16</sup> obtained similar conclusions for various iron nanowire configurations inside armchair nanotubes<sup>16</sup>. On the other hand, work by Kishi *et al.*<sup>17</sup> shows that wires of iron and cobalt lose their magnetic moments when adsorbed on armchair SNWT's. Filling of SWNT's with transition metals has been realised experimentally several years ago<sup>18</sup>, which adds to the potential of these systems. A few studies have been published on electron transport in this context. Iron-SWNT's junctions with C<sub>60</sub> molecules<sup>19</sup> and pristine SWNT's<sup>20</sup> have been proposed as magnetic tunnel junctions. First principles transport calculations yield tunnel magnetoresistances of 11 % and 40 %, respectively, for these systems. A spin-polarised current has also been reported in theoretical works on nanoribbons with substitutional boron atoms<sup>21</sup>, where spin-dependent scattering is found.

Motivated by the reported spin-dependent scattering, we seek here to explain the physical mechanisms found in the numerical calculations. We investigate the influence on the transport properties of a single iron or vanadium atom adsorbed on a SWNT. By performing *ab initio* spin-polarised transport calculations we demonstrate a spin-dependent scattering. The spin type being scattered is shown to depend on the type of adsorbate. By analysing the PDOS of the 3d orbitals of the adsorbates we find the scattering to be caused by coupling of the band states in the SWNT to these orbitals, resulting in Fano resonance phenomena. Using a simple tight-binding model we qualitatively reproduce these results, and also investigate the dependence of the transmission on tube size.

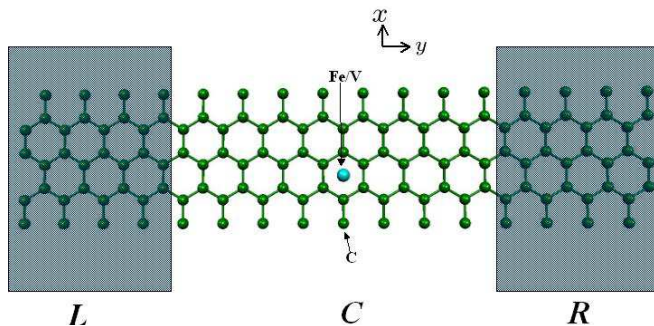


FIG. 1: (Colour online) The unit cell of the system. The sheet is cut in an armchair structure along the  $y$ -direction. The adatom, iron or vanadium is placed in the center. The shaded areas marked  $L$  and  $R$  are the electrodes, and  $C$  is the central region. Periodic boundary conditions are imposed in the transverse direction ( $x$ ).

The paper is organised as follows. Sec. II introduces our model system and the technical details of the calculations. The *ab initio* results are presented in Sec. III and the Fano resonance is briefly introduced along with transmission eigenchannel analysis. In Sec. IV we present a simple tight-binding model which is compared to the *ab initio* results. Results for larger tubes are given based on the simple model.

## II. SYSTEM

The system used for transport calculations is shown in Fig. 1. The graphene sheet is cut in an armchair structure along the  $y$ -direction which results in a metallic system. We employ periodic boundary conditions in the transverse  $x$ -direction. We have used the *ab initio* pseudopotential density functional theory (DFT) as implemented in the SIESTA code<sup>22</sup> to obtain the electronic structure and relaxed atomic positions from spin-polarised DFT. We employ the GGA PBE pseudopotential for exchange-correlation<sup>23</sup>. Our spin transport calculation is based on the nonequilibrium Greens function method as implemented in the TranSIESTA<sup>24</sup> code, extended to spin-polarised systems<sup>25</sup>. However, we only consider here the zero bias limit and focus on electron transmission close to the Fermi energy. According to the TranSIESTA method<sup>24</sup> the system is divided into left and right electrodes, marked  $L$  and  $R$  on Fig. 1, and a central region marked  $C$ . A single iron or vanadium adatom is placed in the middle of the central region. The electrodes both contain 32 atoms while the central region consists of 64 sheet atoms. The adatom systems are relaxed using the CG method with a force tolerance of  $0.01 \text{ eV}/\text{\AA}$ . The carbon atoms were kept fixed during geometry optimisation. The relaxed position of the adatoms is in the center of a hexagon at a distance of  $1.73 \text{ \AA}$  and  $1.89 \text{ \AA}$  from the sheet plane for iron and vanadium, respectively. The pe-

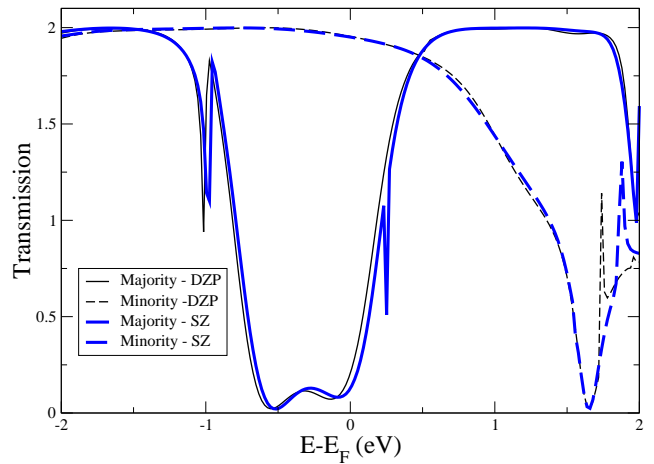


FIG. 2: (Colour online) The transmission of the vanadium adatom system using a single-zeta basis set for the whole system versus using double-zeta polarised for the adatom.

riod of the cell in the transverse  $x$  direction is  $8.52 \text{ \AA}$ , which is then the smallest distance between adatoms in neighbouring cells, and should be enough to prevent significant adatom – adatom interactions. We employ Gamma point sampling ( $k = 0$ ) in the periodic  $x$  direction. The system then corresponds to an  $(2,2)$  armchair nanotube described by the approximate Graphene Sheet Model<sup>26</sup>, that is, neglecting curvature effects. We will return to the dependence of the electron transmission close to the Fermi energy on the GSM-armchair tube width  $(n, n)$  in Sec. IV. The mesh cutoff value defining the real space grid was set to 175 Ry. A single-zeta (SZ) basis set was used. The difference between a SZ basis for all atoms and increasing the vanadium basis to double-zeta polarised (DZP) can be seen on Fig. 2. The only qualitative difference between using DZP and SZ is the additional dip (a single point in the graph) at  $E \approx 0.25 \text{ eV}$  in the SZ case. The reason for this not occurring for DZP is merely a matter of resolution. The dips will be addressed in the following two sections. In the remains of the paper we have used a single-zeta basis.

## III. RESULTS

The spin resolved transmissions as a function of energy relative to the Fermi level,  $E_F$ , of the graphene sheet with iron and vanadium adatoms are shown in Fig. 3. The transmission of a pure sheet is 2 for each spin type, since there are two bands in the energy window each contributing with a fully transmitting channel for each spin. It is seen that spin dependent scattering occurs due to the presence of the adatoms. In the case of iron the minority spin type is significantly suppressed around  $E_F$ , whereas the majority spin electrons transmit completely.

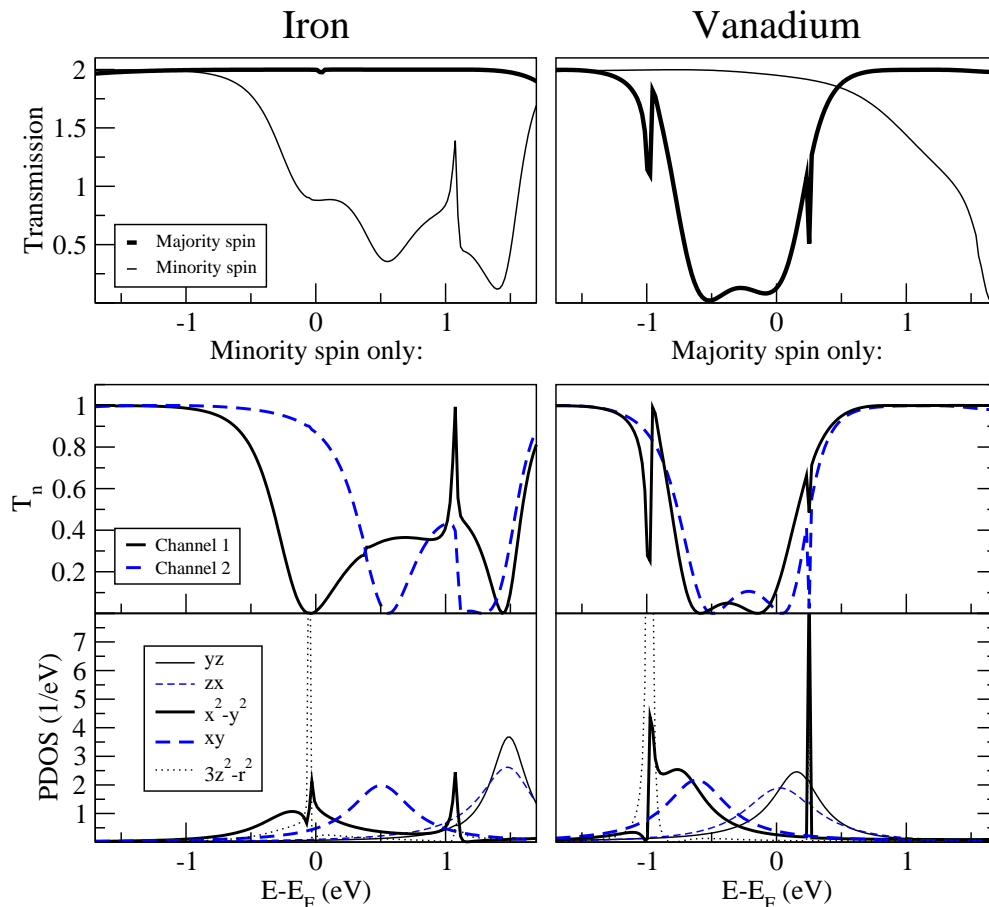


FIG. 3: Top: Transmission as a function of energy for iron (left) or vanadium(right). Within a 0.5 eV range of  $E_F$  the minority spin channels are suppressed in the case of iron whereas the majority channels are suppressed for vanadium. Middle: The transmission of the two minority (majority) spin channels for the iron (vanadium) system. The sum of the two channels yield to total transmission in each case. Bottom: The projected density of states (PDOS) of the 3d orbitals of the iron(vanadium) adatom for minority(majority) spin.

For vanadium, likewise, scattering occurs for only one spin channel, but in this case it is the majority spin electrons which are scattered. The transmission of the two bands for minority (iron) and majority (vanadium) spin is shown on Fig. 3, middle graph. We see that each band closes completely at certain energies.

In the case of vanadium ( $3d^34s^2$ ) we expect from Hund's rules a total spin of 3 and the majority  $d$ -states will be located around  $E_F$ , whereas the minority states are all empty and well above  $E_F$ . The Mulliken analysis indicates a half filling of the majority spin  $3d_{yz}$  and  $3d_{zx}$  orbitals and a full filling of  $3d_{x^2-y^2}$ ,  $3d_{xy}$  and  $3d_{3z^2-r^2}$ . For minority electrons all 3d orbitals are empty. This is in full correspondence with the 3d orbital PDOS plot shown in Fig. 3 bottom graph. In the case of iron ( $3d^64s^2$ ) we expect from Hund's rules that the majority states are all filled and well below  $E_F$ , and now the partially filled minority states are located around  $E_F$  yielding a

total spin of 4. This is again supported by the Mulliken analysis data as well as the projected density of states (PDOS). Comparing PDOS and the transmission there is a strong correlation between adatom orbital energies and conductance dips. This is very clear for the two separated channel closings for vanadium at  $E \approx E_F$  and  $E - E_F \approx -0.5$  eV. The interference between a waves involving the quasi-bound  $d$ -state on the adatom and directly transmitted band states yield a Fano (anti-) resonance. The line shape of the resonance is given by the Fano function<sup>27</sup>

$$f(\epsilon) = \frac{(\epsilon + q)^2}{\epsilon^2 + 1}, \quad (1)$$

where  $\epsilon = (E - E_R)/\Gamma$ . Here  $\Gamma$  is the resonance width,  $E_R$  the resonance energy and  $q$  the asymmetry parameter. Despite the overlapping of dips in our calculations their shape appears symmetric in the vicinity of zero transmis-

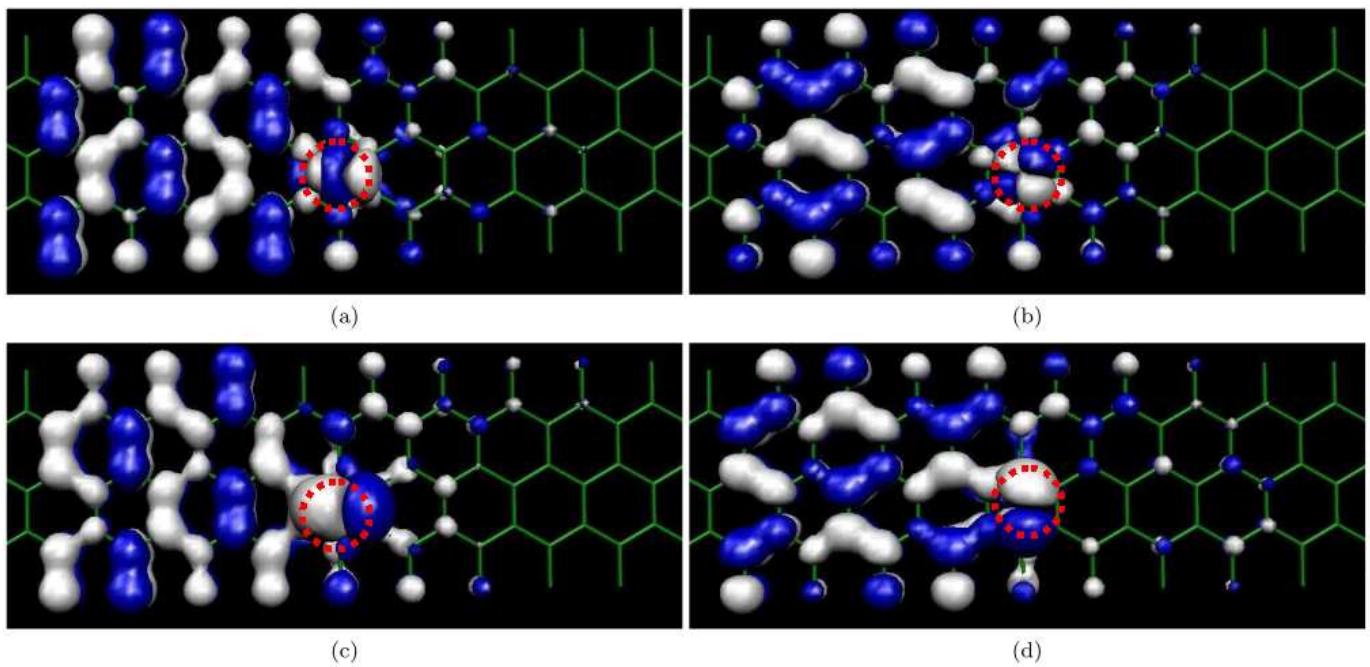


FIG. 4: (Colour online) The real part of the (left-to-right) eigenchannel scattering states for the vanadium system, stemming from majority spin electrons from both bands, at the energy of the first dip (-0.5 eV) (a),(b) and second dip (-0.1 eV) (c),(d) in the transmission spectrum. Only the solutions in the scattering region are shown. The size of the shapes indicates a cut-off value for the wavefunction. White indicates a positive sign a blue a negative sign of the wavefunction. The involved orbitals of the vanadium atom (marked with dotted circle) are seen to be (a) :  $3d_{x^2-y^2}$  (and a minor presence of  $3d_{3z^2-r^2}$ ), (b) :  $3d_{xy}$ , (c):  $3d_{yz}$  and (d) :  $3d_{zx}$ .

sion. Since the structure has inversion symmetry around the adatom in the transport direction the parameter  $q$  must be real and thus we expect to have zero transmission dips as seen in Fig. 3 at the anti-resonances  $\epsilon = -q^{28,29}$ . A very sharp resonance can be seen for vanadium around  $-1\text{eV}$  which should also go to zero. However, it is related to the most localized  $d$ -orbital,  $d_{3d^2-r^2}$ , and a small asymmetry in the numerical calculation and the resolution cause it not to go exactly to zero. Signatures of Fano resonances have previously been observed experimentally in the conductance of multi-wall carbon nanotubes at low temperature<sup>30</sup>.

The anti-resonances are illustrated further by performing an eigenchannel analysis where scattering states with well-defined transmissions ("eigenchannels") are constructed<sup>31</sup>. We take vanadium as our example. The eigenchannel transmissions,  $T_n(\epsilon)$ , provide the transmission of channel  $n$  at a given energy  $\epsilon$ . Plotted on Fig. 4 (a)(b) and (c)(d) are the real part of the majority spin scattering state solutions of both bands for energies corresponding to the first dip ( $-0.5\text{eV}$ ) and the second dip ( $-0.1\text{eV}$ ), respectively. We see that the wavefunction is nonvanishing only on the left side of the vanadium atom as expected since we have full reflection in all cases. The anti-symmetric and symmetric solutions are seen on Fig. 4 (a)(d) and (b)(c), respectively. Note that in the transverse direction the neighbouring C

atoms have the same (opposite) sign in the symmetric (anti-symmetric) case. These solutions are indeed matched by the vanadium atom orbitals, which is seen on the figures by a match of signs (colours). From the shape and sign in the plots the orbitals involved can be identified for each band at both energies.

#### IV. A TIGHT-BINDING MODEL

We will now rationalize the results for the channels and transmissions in terms of the simplest possible tight-binding model. We consider only the coupling of the adatom  $d$ -orbitals with the 6 nearest  $\pi$ -orbitals. The starting point will be the two band states of the  $\pi$ -electrons in the armchair direction at the Fermi level, see Fig. 5. These are characterized by rotational symmetry around the tube axis and come in an odd/even version around the symmetry plane normal to  $x$  along the tube ( $y$ ) and cutting through the adatom. They couple to different  $d$ -orbitals on the adatom with the same symmetry. Thus the symmetric/anti-symmetric band only couple to the  $d$ -orbitals even/odd in  $x$ . To make a minimal model (with a minimum of parameters) we assume that the  $d$ -orbitals have the same on-site energy  $E_d$ , and a coupling to the carbon  $\pi$ -orbitals described in units of

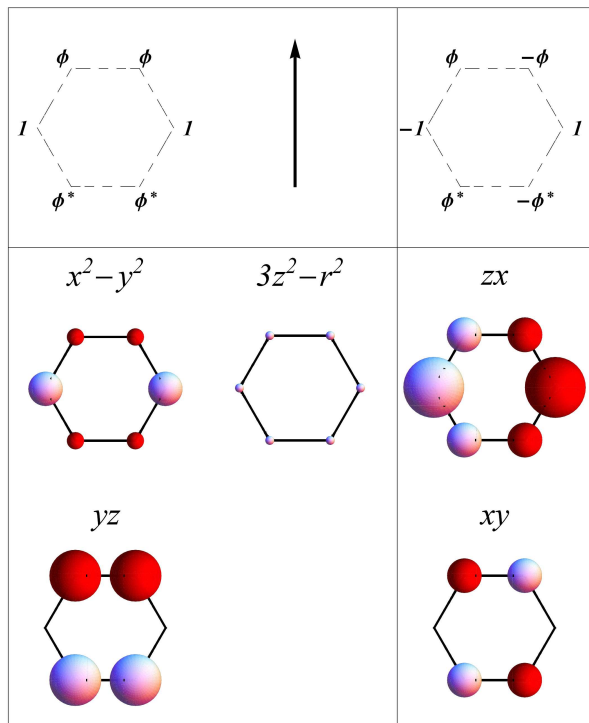


FIG. 5: (Colour online) Top panel: The two  $\pi$ -band ( $p_z$ ) states (not normalized) in a hexagon where the arrow denotes the direction along the armchair tube ( $y$  direction) with  $\phi = e^{i2\pi/3}$ . Left/right panel correspond to symmetric/anti-symmetric solution on the A,B-dimers ( $x$  direction). Lower panels: Simple tight-binding model. The sign and relative size of the hopping matrix elements between the ring  $\pi$ -orbitals and the metal adatom  $d$ -orbitals when the metal-atom is situated  $1.7\text{\AA}$  above the middle of the ring.

$V_{pd} = V_{pd\sigma}$  taking  $V_{pd\pi} \approx 0.5V_{pd\sigma}$ <sup>32</sup>. The size and sign of the coupling of the different  $d$ -orbitals to the  $p_z$  orbitals are illustrated in Fig. 5, left/right panels corresponding to coupling to the two types of bands. For both bands it is seen that the  $d_{3z^2-r^2}$  orbitals do not couple at  $E_F$  since the wavefunction values around the hexagon sums up to zero. Therefore we do not expect significant contributions from this orbital, which will be very localised.

We only consider the majority spin  $d$ -states for V, since they, as mentioned above, will be located around  $E_F$  with  $E_d \approx 0$ . Likewise, for iron we only consider the minority spin states. The model calculation with  $(E_d, V_{pd})$  parameters chosen to fit the data from the full *ab initio* calculation are shown in Fig. 6. It is seen that the transmission is more suppressed in the full calculation where the individual  $d$ -orbitals are allowed to have different energies, but the fact that we see 4 dips corresponding to the four coupling  $d$ -orbitals is clear.

With the simple model we can now explore what happens when the diameter of  $(n, n)$ -tube is increased. This is shown in Fig. 7 where it is seen that the transmission still goes to zero at the anti-resonance points but

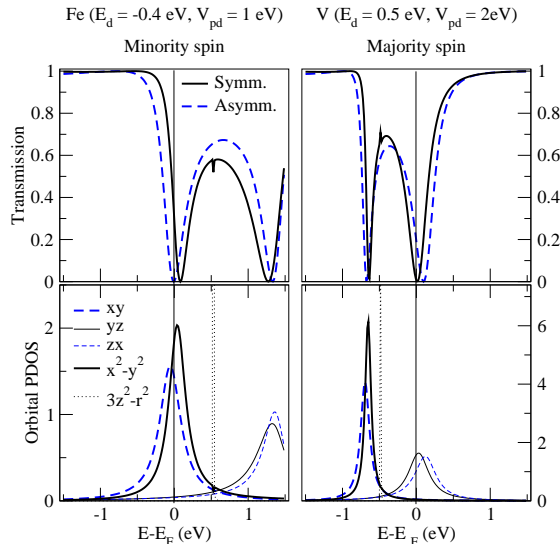


FIG. 6: (Colour online) The transmission through the symmetric/anti-symmetric bands for Fe minority spin (left panels) and V majority spin (right panels) calculated with the simple tight-binding model. Lower panels display the projected density of states onto the  $d$ -orbitals.

in an interval getting narrower with increasing  $n$ . The latter is in agreement with the findings of Todorov and White<sup>33</sup>. They conclude that the larger the tube diameter the more the scattering due to an impurity is reduced. This happens because the overlap with the wavefunction (normalised around the tube circumference) with the scattering potential goes down. The fact that the conductance still drops to zero in our calculations is due to the Fano resonance phenomena.

## V. CONCLUSION

We have described spin-polarised zero bias transport calculations for armchair carbon nanotubes with adsorbed single iron or vanadium atoms. We find a significant difference between transmissions of majority and minority spin. The presence of the metal adatoms causes spin-dependent closing of the conduction channels at certain energies. The mechanism is due to Fano resonances related to the particular  $d$ -states close to the Fermi energy. Only  $d$ -orbitals with a symmetry matching the symmetry of the Bloch band solutions take part in the scattering. The scattered spin type (minority or majority spin) can be explained by the filling of the  $3d$  orbitals via Hund's rule. Results of a simple tight-binding model show that increasing the width of the tube, and thus reducing the concentration of adatoms, results in narrower dips in the conduction, but still with complete closing. The latter is explained by the reflection symmetry of the system in the transport direction.

## Acknowledgments

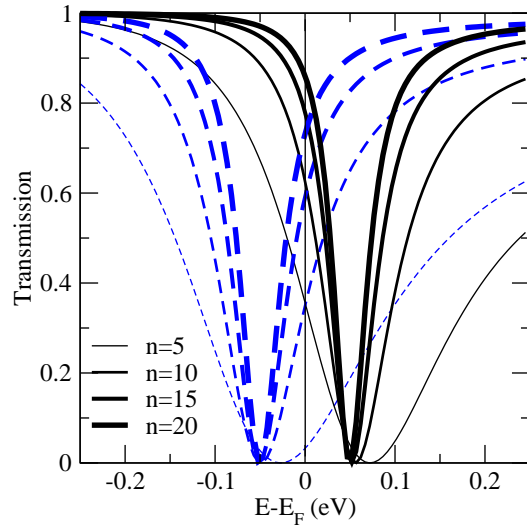


FIG. 7: (Colour online) The dependence on tube-size,  $(n, n)$  calculated with the simple tight-binding model at the first dip in the Fe case.

The authors would like to thank Jeremy Taylor for useful discussions. Computational resources were provided by the Danish Center for Scientific Computations (DCSC). APJ is grateful to the FiDiPro program of the Finnish Academy for support during the final stages of this work.

---

\* Corresponding author: jof@mic.dtu.dk

---

- \* Corresponding author: jof@mic.dtu.dk
- <sup>1</sup> P. Avouris, Z. Chen, and V. Perebeinos, *Nature Nanotechnology* **2**, 605 (2007).
  - <sup>2</sup> A. Geim and K. Novoselov, *Nature Materials* **6**, 183 (2007).
  - <sup>3</sup> G. Prinz, *Science* **282**, 1660 (1998).
  - <sup>4</sup> S. Wolf, *Science* **292**, 1488 (2001).
  - <sup>5</sup> I. Zutic, J. Fabian, and S. Das Sarma, *Rev. Mod. Phys.* **76**, 323 (2004).
  - <sup>6</sup> P. Lehtinen, A. Foster, Y. Ma, A. Krasheninnikov, and R. Nieminen, *Phys. Rev. Lett.* **93**, 187202 (2004).
  - <sup>7</sup> H. Kumazaki and D. S. Hirashima, *Journal of the Physical Society of Japan* **76**, 64713 (2007).
  - <sup>8</sup> E. J. Duplock, M. Scheffler, and P. J. Lindan, *Phys. Rev. Lett.* **92**, 225502 (2004).
  - <sup>9</sup> S. Okada and A. Oshiyama, *Phys. Rev. Lett.* **87**, 146803 (2001).
  - <sup>10</sup> H. Lee, Y.-W. Son, N. Park, S. Han, and J. Yu, *Phys. Rev. B* **72**, 174431 (2005).
  - <sup>11</sup> B. Fagan, R. Mota, A. da Silva, and A. Fazzio, *Physica B* **340**, 982 (2003).
  - <sup>12</sup> B. Fagan, R. Mota, A. da Silva, and A. Fazzio, *J. Phys.: Condens. Matter* **16**, 3647 (2004).
  - <sup>13</sup> S. B. Fagan, R. Mota, A. J. R. da Silva, and A. Fazzio, *Phys. Rev. B* **67**, 205414 (2003).
  - <sup>14</sup> D. Duffy and J. Blackman, *Phys. Rev. B* **58**, 7443 (1998).
  - <sup>15</sup> C.-K. Yang, J. Zhao, and J. P. Lu, *Phys. Rev. Lett.* **90**, 257203 (2003).
  - <sup>16</sup> Y.-J. Kang, J. Choi, C.-Y. Moon, and K. Chang, *Phys. Rev. B* **71**, 115441 (2005).
  - <sup>17</sup> T. Kishi, M. David, A. Wilson, H. Nakanishi, and H. Kasai, *The Jap. Journal of Appl. Phys.* **46**, 1788 (2007).
  - <sup>18</sup> M. Monthieux, *Carbon* **40**, 1809 (2002).
  - <sup>19</sup> C. Zhang, L. Wang, and H. Cheng, *The Journal of Chem. Phys.* **124**, 201107 (2006).
  - <sup>20</sup> B. Wang, Y. Zhu, W. Ren, J. Wang, and H. Guo, *Phys. Rev. B* **75**, 235415 (2007).
  - <sup>21</sup> T. Martins, R. Miwa, A. da Silva, and A. Fazzio, *Phys. Rev. B* **98**, 196803 (2007).
  - <sup>22</sup> J. M. Soler, E. Artacho, J. D. Gale, A. Garcia, J. Junquera, P. Ordejon, and D. Sanchez-Portal, *Journal of Physics-Condensed Matter* **14**, 2745 (2002).
  - <sup>23</sup> J. P. Perdew, K. Burke, and M. Ernzerhof, *Phys. Rev. Lett.* **77**, 3865 (1996).
  - <sup>24</sup> M. Brandbyge, J.-L. Mozos, P. Ordejon, J. Taylor, and K. Stokbro, *Phys. Rev. B* **65**, 165401/1 (2002).
  - <sup>25</sup> S. Datta, *Electronic Transport in Mesoscopic Systems* (Cambridge University Press, Cambridge, England, 1997).
  - <sup>26</sup> C. T. White and J. W. Mintmire, *Journal of Physical Chemistry B* **109**, 52 (2005).
  - <sup>27</sup> U. Fano, *Phys. Rev.* **1**, 1866 (1961).
  - <sup>28</sup> J. U. Nockel and A. D. Stone, *Phys. Rev. B* **50**, 17415 (1994).

- <sup>29</sup> A. R. P. Rau, *Physica Scripta* **69**, C10 (2004).
- <sup>30</sup> Z. Zhang and V. Chandrasekhar, *Phys. Rev. B* **73**, 075421 (pages 10) (2006).
- <sup>31</sup> M. Paulsson and M. Brandbyge, *Phys. Rev. B* **76**, 115117 (2007).
- <sup>32</sup> W. A. Harrison, *Electronic Structure and the Properties of Solids* (Dover, 1989).
- <sup>33</sup> C. T. White and T. N. Todorov, *Nature* **393**, 240 (1998).